ANALYSIS OF SHIP/PLATFORM IMPACTS

T.H. Søreide T. Moan J. Amdahl J. Taby
The Norwegian Institute of Technology, Trondheim, Norway

SUMMARY

The paper deals with ship collision against platform. A general description of the collision mechanisms is given and various methods available for analyzing the collision problem are discussed. Models of energy absorption of steel platforms are identified and compared.

Simple computer programs based on plastic yield line theory has been developed for the analysis of local energy absorption, i.e. energy associated with deformation work in the vicinity of the point of impact. For studying energy absorption by beam bending of the impact element between adjacent joints yield hinge models accounting for axial restrictions as well as F.E.M. programs are applied. Constraints on the energy absorbing capability caused by local buckling, ovalization and tubular joint capacity are discussed.

Theoretical load-deformation predictions derived from the methods above are compared with experimental results from local denting and global bending of small scale tube models, showing reasonably well agreement.

The results of an introductory study with axial crushing of radially stiffened cylinders are presented with special reference to ship deformation characteristics in bow and stern collisions.

Comparison is given between analytical models and experiments on axial capacity of dented tubes. The main theory behind an efficient computer program for predicting post-damage strength of tubular members is described.

1. INTRODUCTION

Many types of steel structures which are employed in the offshore petroleum activity are composed of tubular members. These structures are subjected to various types of loads. Besides the normal functional loads and environmental loads, loads due to accidental events such as collisions, falling objects might occur. Statistics for world wide operation platforms during 1/1-70 to 31/12-80 indicate 9 cases with total or severe damage of the platform among 114 incidents with similar result /1/. At the same time many impact incidents with minor consequences have been reported. As the number and size of vessels used in offshore operations (especially in the North Sea) increase, the collision risk should be seriously considered in the design of platforms. It is therefore of interest to assess the damage caused by such loads.

Furthermore, both in connection with design and operation it is of interest to know the residual strength of a structure damaged due to accidental or other types of loads. During operation such knowledge is necessary to make decision regarding repair in order to balance the costs and safety.

This paper presents recent findings regarding the structural behaviour during impact between ships and unstiffened tubular members of an offshore platform. In Chapter 2 the fundamental impact mechanics is briefly summarized. Chapter 3 is devoted to the load-deflection characteristics of tubular members and ship-bows necessary to determine the maximum impact force and/or damage. In Chapter 4 the problem of residual strength of a damaged tubular member is addressed.

2. IMPACT MECHANICS

The derivation of a mathematical model of the ship/platform impact is based on two criteria

- the energy conservation law
- force equilibrium

The condition of energy conservation is expressed by the following equation for collision against a fixed platform

$$E_k = E_s + E_p + E_f + E_r \qquad (1)$$

where

E_k = kinetic energy of the striking vessel immediately before impact

E_s = energy absorbed by ship

E_p = energy absorbed by platform

E_f = energy absorbed by fenders

E_r = rotational kinetic energy of the ship after impact

In case of eccentric impact some of the kinetic energy may remain as rotational energy of the ship after impact. For design purposes the worst case is a central impact which means that the line through the centre of gravity of the ship and the contact point coincides with the direction of ship motion.

For an unfendered structure the two last terms of Eq. (1) disappear and the energy conservation condition comes out as:

$$\tfrac{1}{2}mv_0^2 = E_s + E_p \qquad (2)$$

where

m = mass + added mass of ship

v_0 = impact velocity

Force equilibrium is fulfilled simply by assuming that the same force P is acting in each medium. Given the load-deformation characteristics for ship and platform it is possible to calculate the energy absorption at different load levels satisfying force equilibrium.

The choice of design impact situations must be done under the consideration of probability of occurrence /3/. The size of the design vessel is to be determined on the basis of the vessels intended to operate in the area such as service vessels, tankers for offshore loading and by-passing ships. The usual criterion is to consider a supply vessel drifting sideways and causing a central impact on the platform.

3. LOAD-DEFORMATION CHARACTERISTICS OF PLATFORM BRACING AND SHIP BOW

3.1 Energy Absorption in Platform Bracing

The deformation modes of the platform at impact may conveniently be categorized as

- local deformation of bracing/leg at point of impact
- global beam deformation of bracing and leg element
- overall deformation of platform

The transition between local and global deformation of a bracing element is difficult to set. As a dent is created in the tube wall the neutral axis changes, a phenomenon that is more associated with global beam deformation. While the two first modes involve considerable plastic energy absorption, the global response is mainly elastic, possibly involving some dynamic effects.

3.1.1 Local Deformation of Tube Wall

The extent and form of local damage in the wall of a bracing element depends on the nature of impact. A head-on collision gives a more concentrated force than a sideways impact and results in a larger amount of local energy absorption for given mass and velocity of the vessel. Due to this complexity it is impossible to present one single analytical model for establishing local energy absorption. Several types of models have to be considered related to different collision cases.

For sideways impact a simple yield line model is presented by Furnes and Amdahl /3/, see also Fig. 1. The deformed surface is bounded by a series of yield lines and the following plastic effects are included

- rotation of surface at yield lines
- flattening of surface between yield lines
- tension work due to elongation of generators

The theoretical model gives fairly good agreement with experimental results for small and medium indentations. The model can form the basis for possible design curves when further verification against experiments has been performed.

3.1.2 Analytical Techniques for Beam Deformation of Bracing Element

The rigid-plastic methods of analysis /4, 5/ provide simple analytical results, often with acceptable accuracy and are appropriate for design situations. The simplest approach to the beam type of deformation is the three hinge mechanism, Fig. 2. In case of axially restrained ends the load carrying capacity of the beam increases considerably as the beam undergoes finite deflections due to the development of membrane tension forces. For a centrally loaded tubular beam the load-deflection relation is given by /4/

$$\frac{P}{P_0} = \sqrt{1 - \left(\frac{w}{D}\right)^2} + \frac{w}{D}\arcsin\frac{w}{D}; \quad \frac{w}{D} \leq 1 \tag{3}$$

$$\frac{P}{P_0} = \frac{\pi}{2}\frac{w}{D} \quad ; \quad \frac{w}{D} > 1 \tag{4}$$

where w is the central deflection at the point of impact and D is the tube diameter. P_0 is the plastic collapse load according to linear yield theory.

The above expressions are based on the assumption that the ends have full axial restraint. In a real frame system like a jacket the bracing element sustains a certain degree of elastic support from the adjacent elements. Besides, local deformations occur in the tubular joints. Such elastic restrictions can be included by extending Hodge's method /6/ for the case of tubular members.

It is a major requirement for the validity of the present simple theory that no buckling of the tube wall takes place so that the full plastic capacity of the cross section is retained during deformation. Thus, restrictions must be set on maximum D/t-ratio for which the rigid-plastic theory can be used. Sherman /7, 8/ on the basis of tests on steel tubes in bending concluded that for members with D/t of 35 or less the full plastic moment is activated and sustained during deformation.

The API rules /9/ prescribe $D/t < 9000/\sigma_y$ (σ_y in N/mm^2) to maintain full capacity through plastic deformation. In the range $9000/\sigma_y < D/t < 15200/\sigma_y$ only a limited plastic rotation capacity can be presumed.

For the clamped ideally plastic element the absorbed plastic energy at any level of deflection w is found by integration of the load-displacement expressions in Eqs. (3, 4). The following energy expression

$$E = P_0 D\{\frac{3}{4}\frac{w}{D}\sqrt{1 - \frac{w^2}{D^2}} + \frac{(1+2\frac{w^2}{D^2})}{4}\arcsin\frac{w}{D}\}; \quad \frac{w}{D} \leq 1 \tag{5}$$

$$E = \frac{\pi}{8}P_0 D(1+2\frac{w^2}{D^2}) \quad ; \quad \frac{w}{D} > 1 \tag{6}$$

3.1.3 Computational Techniques for Bracing Elements

In an effort to come up with an efficient tool for collision analysis of bracing elements a simple finite element beam program IMPACT has been modified to take care of local effects such as moment capacity reductions due to indentation and buckling of tube wall.

The deformation model at the point of impact is shown in Fig. 3. It is assumed that the indented area is flat and that the remaining part of the cross section has constant radius of curvature. The shape of the cross section can now be determined for any indentation by requiring the area to be constant and the reduced plastic section modulus comes out from simple integration over the deformed cross section. The beam elements at point of impact are modified continuously during deformation so as to satisfy this reduced plastic moment capacity.

In order to calculate the amount of indentation at different load levels, the technique described in Sect. 3.1.1 is applied. The program system now consists of three integrated parts

- a finite element beam program with elasto-plastic material behaviour and large deflection effects incorporated
- a yield line program for predicting local indentation
- a program for calculating reduced moment capacity due to local deformation at point of impact

The load is applied in increments with equilibrium interaction within each load step. A further documentation of the numerical technique is found in Ref. /10/.

In order to simulate the real deformation pattern in the tubular member a full shell analysis must be performed in which material as well as geometric nonlinearities are incorporated. Fig. 4 shows the finite element model of a bracing element analysed by the computer program TUBB /11/. In the central region close to the point of impact a fine mesh of triangular thin shell elements is used while the tube wall outside the local indentation area is represented by a coarser mesh of rectangular elements. The total number of elements is 370.

Strain hardening is accounted for by combining the socalled sublayer technique with the flow theory of plasticity. Geometric nonlinaritiy is modelled by the updated Lagrangian formulation /10/ in which element strains are referred to local element axes.

The displacement pattern along the bracing and deformation of midsection are shown in Fig 5 as calculated by TUBBUC and the corresponding load/displacement curve is illustrated in Fig. 6 The stiffening effect of membrane forces is clearly demonstrated.

It is clear that the above technique is time consuming and costly. For design purposes a simpler numerical tool should be available. However, modification of the computational method also reduces the accuracy of the predictions. The shell program can be used to study special effects in the member performance eg. stress distribution close to the point of impact and local instability phenomena.

3.1.4 Behaviour of Tubular Joints

A major condition for the validity of the above models is that the restraints from the joints on the bracing elements can be incorporated. In the elastic regime the linear stiffness of the joint can be calculated by shell programs for different load cases such as axial tension, axial compression, in-plane bending and out-of-plane bending. The finite element beam program of Sect. 3.1.1 is modified so as to take in translational and rotational springs at the ends of each element.

However, in order to simulate the energy absorption under extreme loading it is also essential to model the nonlinear load-deformation characteristics of the joints. Further, failure criteria for tubular joints should be given as deformation limits for the springs. Typically, a joint subjected to bending may fail by buckling of the chord wall on the compression side resulting in a reduction in joint stiffness and strength. On the tension side fracture through the chord wall is the most probable mode of failure. It is clear that the combination of membrane forces and moments at the ends of the tubular elements should be checked against empirical data on tubular joint capacity. The simplest alternative is to use springs for which the load-deformation characteristic is given as input, either in the form of an ideal elasto-plastic type of relation or a general nonlinear curve including unloading in the plastic regime.

Valuable information on the nonlinear behaviour of unstiffened tubular joints has been presented by Yura et al. /12/. Capacity formulas based on experimental data are also given in design codes /9, 13/.

3.1.5 Laboratory Tests of Bracing Elements

The experiments presented are part of a series of tests performed to study the energy absorption capability and post-damage strength of tubular members. Characteristic cross-sectional dimensions of bracing elements in the water plane are

$$1.0 < D < 2.0 \text{ m}$$
$$20 < D/t < 100$$
$$10 < L/d < 30$$

In the study of impact capability of bracing elements two series of tests were performed, namely with no axial restraint at the ends and with horizontally fixed ends. In both cases the specimens were clamped against rotation. Strain gauges were placed at point of impact and at the ends in order to get information about the very complicated deformation patterns in these areas. Extensiometers recorded horizontal movements at the ends and lateral deflection of tube wall in top and bottom of the central cross section.

Geometric and material data for the models are given in Table 1. The range of variation is

$$63 < D < 125$$
$$22 < D/t < 61$$
$$10 < L/D < 20$$
$$204 < \sigma_Y < 328 \text{ N/mm}^2$$

Displacement control of the hydraulic jack was applied with a displacment rate of 0.15 mm/sec. for the quasi-static tests and 54 mm/sec. for the dynamic tests.

For a more detailed description of the experiments, see Ref. /14/. A short presentation of the most interesting results will be given here.

First, attention is given to the effect of membrane forces by considering the two specimens IAI and IAIII with equal geometric and material properties. Specimen IAI has horizontally free end conditions and IAIII is clamped against axial movement. The corresponding load-displacement curves are given in Fig. 7, where comparison is made with simple mechanism theory and with computer predictions by the modified beam program of Sect. 3.1.3. The effect of membrane forces is clear in the post-collapse domain of deformation. For specimen IAI the experiment gave a drop in lateral load in the plastic region. This phenomenon is due to a reduction in moment capacity at the ends caused by local crippling of the compression side of the tube wall, Fig. 8. For case IAIII the membrane tension field prevents this type of local damage. Instead, the ends of IAIII fail by fracture close to the weld, Fig. 9.

The stretching effect of membrane forces is also illustrated by the pictures in Fig. 10 and 11. The ovalization of the tube is of a much more local character for IAI than the overall deformation of IAIII.

The conclusion to be drawn is that the modified beam computer program predicts well the load-displacement characteristics. The simple mechanism theory gives too high capacity at small deflections due to the neglection of local deformation at point of impact. For large deflections the mechanism model is conservative neglecting the effect of strain hardening.

3.2 Energy Absorption in Ship Bow

The configuration of a ship structure is very complex, being comprised of an outer shell stiffened by a grid of stringers, frames and profiles. In a collision, the interaction between the ship and the platform may cause a complicated deformation pattern with cutting, puncturing and rupture of both structures. At the Division of Marine Structures, NTH, a series of tests on small-scale models of ship bows is presently conducted, in close cooperation with Det norske Veritas.

In this section some introductory experiments with ring-stiffened cylindrical shells are reported. Bulbous bows bear some resemblance to simple cylindrical shell. In a collision with a concrete tower of a platform or a bridge pier it is likely that the bulb will suffer the greater part of the deformation. Thus axial compression tests with cylindrical shells provide valuable information with regard to the properties of bulbs.

3.2.1 Shell Buckling

The initial buckling phase of deformation contributes to a minor extent to the energy absorption of the cylinder. However, the buckling mode may predict the type of plastic mechanism. In most cases the buckling mode develops further into the plastic regime and forms the energy absorbing mechanism. Thus, it is of great importance in the study of energy absorbing capability of cylindrical shells also to predict the initial buckling mode.

The elastic buckling behaviour of a ring-stiffened cylindrical shell may conveniently be related to the Batdorf-parameter /15/

$$Z = \frac{\ell^2}{Rt}\sqrt{1 - \nu^2} \tag{7}$$

where ℓ is the stiffener spacing, R is radius of cylinder and t is wall thickness, see also Fig. 12.

For cylindrical shells under axial loading and bending shape imperfections may significantly reduce the elastic buckling stress. Thus the critical stress according to classical shell buckling theory should be reduced by a knockdown factor as given by design rules /13/.

3.2.2 Plastic Collapse Models

After initial buckling the shell continuous to deform into the plastic regime. The post-buckling behaviour may take on two forms, one with the shell in axisymmetric convolutions, the other in which asymmetric folds are developed.

The analysis is carried out by assuming the mode of collapse of the tube and calculating the initial work required to achieve this mode. Equating this work to the external work the mean collapse load is derived. To simplify the analysis elastic strains are neglected and initially a rigid-plastic material without strain hardening is assumed. The axisymmetric collapse model is shown in Fig. 13.

There are two contributions to the internal energy absorption; namely the work associated with bending at the hinge lines and stretching in the circumferential direction, respectively.

According to Alexander /16/ the average collapse load is given by the expression

$$P_{av} = \frac{\pi\sigma_y t^2}{\sqrt{3}}\left(3.3\sqrt{\frac{D}{t}} + 1\right) \tag{8}$$

where D and t is the shell diameter and thickness respectively.

It is interesting to note that the plastic buckling half length given by

$$h = 0.953\sqrt{Dt} \tag{9}$$

is quite close to the elastic buckling length /15/.

$$h' = 1.22\sqrt{Dt} \tag{10}$$

Fig. 14 shows that the theoretical plastic collapse load approaches infinity with the formation of a new fold. However, in practice the load level is limited by the initial buckling strength of the cylinder wall.

The mechanism mode of the asymmetric collapse mode shown in Fig. 15, is comprised of a grid of hinge lines in which angular rotation is concentrated. The tube surface is transformed into plane triangles. In this mode there is no stretching of the material around the circumference in the axial direction. The following terms contribute to the internal energy absorption

- removal of shell curvature
- bending about horizontal yield lines
- bending about oblique yield lines
- travelling horizontal yield lines

The last term derives from the assumption that a new buckle is created by a horizontal hinge travelling down from the last hinge to the position of the new one. During this cycle the material is bent and rebent in the hinge line.

The average collapse load according to Johnson et al /17/ reads

$$\bar{P}_{av} = \frac{2\pi M_p}{1-2\frac{r}{h}}\left(1 + \frac{n}{tg(\frac{\pi}{2n})} + \frac{n}{\sin(\frac{\pi}{2n})} + \frac{D}{r}\right) \qquad (11)$$

where n is the number of triangles around the circumference, D is the shell diameter, r is the rolling radius of travelling yield lines and M_p is the plastic moment of the shell pr. unit width.

The unknown rolling radius r can be found formally by minimizing the load with respect to r. The load decreases with decreasing n. However, the number of circumferential waves is influenced by the initial buckling pattern.

In real collisions the strain rate sensitivity of the yield stress may be of great importance for the energy absorption in steel members. Static considerations of impacts may highly underestimate the energy absorption capability.

A simple method of including the dynamic material behaviour is to adjust the yield stress value according to the average strain rate $\dot{\varepsilon}$. The following power type formula has been suggested by Cowper and Symonds /18/

$$\frac{\sigma_y'}{\sigma_y} = 1 + \left(\frac{\dot{\varepsilon}}{\dot{\varepsilon}_0}\right)^{\frac{1}{n}} \qquad (12)$$

where $\dot{\varepsilon}_0$ and n are material constants determined to get the best fit of experimental data. Recommended values for mild steel are $\dot{\varepsilon}_0 = 40\ \text{sec}^{-1}$ and n = 5.

The average strain rate in the shell wall may be approximated by /19/

$$\dot{\varepsilon} = \frac{\dot{u}t}{4hr} \qquad (13)$$

where $\dot{u}$ is the loading velocity, t is the wall thickness, h is the half-length of the buckling wave (=ℓ/2) and r is the radius of rolling.

The present experiments indicate t/r around 1.0. Thus, Eq. (13) simplifies to

$$\dot{\varepsilon} = \frac{\dot{u}}{4h} \qquad (14)$$

which is used in subsequent calculations of test models.

3.2.3 Experiments

The series of collision tests with axially loaded cylindrical shells contains ten specimens, four of which are machined and six fabricated cylinders. The four machined shells have been tested to initial buckling /20/ and in the present study they are plastically compressed to total collapse. The specimens are machined from 12 mm thick seamless tubes that are stress relieved before being machined. These cylinders are almost ideal in the sense that residual stresses and shape imperfections are small. In the subsequent text these machined specimens are denoted MA1-MA4.

The six fabricated cylinders are rolled from 2 mm plate, and then closed by a longitudinal butt weld. The ring stiffeners are machined from 25 mm seamless tubes and attached to the shell by intermittant fillet welds. After welding the cylinders are stress released by heating to 550-600°. In the following, these fabricated models are denoted FA1-FA6.

The diameter is 400 mm for all cylinders. Data for thickness, stiffener spacing and yield stress are given in Table 2. The initial bukcling stresses are presented in Table 3.

The initial buckling stresses are presented in Table 3.

Comparison is made with theoretical elasto-plastic buckling stresses. It is seen that the analysis underestimates the capacity of the machined models. One major reason for this result is that they are almost ideal specimens as far as shape imperfections and residual stresses are concerned. The two specimens FA1 and FA5 are seen to have test results considerably below the analytical prediction. The low experimental stresses are caused by difficulties arising during the loading of FA1 and FA5. Strain measurements around the cylinders indicated a skew load distribution coming from inaccuracy in the end geometries of the two specimens. However, in the subsequent plastic deformation the specimens FA1 and FA5 behave normally.

The low R/t ratio of 100 for the fabricated models implies low sensitivity for shape imperfections. Thus, the four successful models FA2, FA3, FA4, and FA6 have buckling stresses considerably higher than predicted.

The conclusion from the present study of initial buckling is that the theory of sec. 3.3.1, which forms the basis of the DnV rules of 1977 /11/ seems to include a reasonable degree of safety. However, it should be emphasized that more and larger-scale tests have to be performed before any clear conclusion can be drawn. The buckling tests of Odland /20/ give a more reliable basis for such considerations.

An example of a measured load axial displacement curve in the plastic collapse phase is shown in Fig. 16. The shape of the curve is explained by the development of plastic mechanisms. The initial buckling implies axisymmetric deformation of the cylinder wall between two stiffeners. A sudden drop in the axial load is observed after the initial buckling. During continuing axial compression this region deforms. The load drops to a minimum and rises again until two stiffeners overlap and a new region buckles. Due to the shape disturbances from the collapsed region, the successive buckling loads are much lower than the initial one.

The successive development of axisymmetric plastic mechanisms is also illustrated by the pictures in Fig. 17. Fig. 18 shows the plastic deformation of specimen FA6 for which four asymmetric folds are developed around the circumference.

In order to check the validity of the proposed mechanism theory it is convenient to compare the average collapse load P_{av} with the experimental values. The latter are found by numerical integration of the load/displacement curves. Because of hardening effects during plastic deformation an average value of the uniaxial tensile stress is introduced as characteristic yield stress.

Table 4 indicates some discrepancy between analytic predictions and test results. In all cases the experimental values lie above the analytical predictions. Several factors can explain this discrepancy.

First, the deformation patterns in the tests differ somewhat from the configurations assumed in the mechanism models. For the machined models the ring stiffeners are rather weak so that they undergo twisting. The deformed stiffeners prevent the development of an ideal mechanism in the shell wall.

The second effect of importance is that in the theoretical models the plastic hinges are supposed to be stationary. However, during the tests it is easily observed that the location of plastic zones changes during deformation. Such a motion of plastic hinges gives an extra contribution to plastic energy absorption and thereby raises the average load P_{av}. The theoretical models do not account for this effect.

The choice of realistic yield stress to be used in the capacity formulae is another factor of uncertainty. The yield stress σ_y is modified for plane strain conditions and material hardening. The question is how good these approximations are, and above all, how representative are the uniaxial tensile tests for describing the material behaviour in the shell wall.

3.2.4 Analysis of Bulbous Bow

Among the variety of shapes, bulbs may also take on a cylindrical cross-section, thus showing great similarity to the tested cylindrical shells. However, there is one important difference. In addition to transverse frames, the bulbs normally also contain a longitudinal stiffening system, consisting of stringers and a centerline bulkhead. This will, indeed, influence the deformation pattern as well as the energy absorption of the bulb. For the time being, the effects of the stringers and bulkheads can be included in a simplified and inaccurate way. This fact must be taken into account when evaluating the results.

Unfortunately, there are very little data available on the crushing strength of bulbs. The only information is provided by the tests conducted by Woisin /21/. Some of these tests involved the bow model of the 195,000 dwt. tanker "Esso Malaysia" to scale 1:12 and the side barrier of a nuclear ship. The barrier was of a resistance type, confining almost all damage to the bow structure. In one of the tests only the bulb part of the bow suffered the deformation.

The force-deformation relationship of this test, derived from the acceleration recordings, is reproduced in Fig. 19 /22/. The absorbed energy, found by integrating the load curve, comes out to be 28% less than the initial ramming energy applied in the test, indicating that the acceleration measurements were inaccurate. In the same diagram the load prediction by means of Gerard's method is depicted /23/. In this procedure the cross-section is cut into simple elements for which the crippling strength is determined on the basis of experimental data from the aerospace industry.

From Fig. 19 it is seen that Gerard's method agrees reasonably well with tests measurements while the yield line theory underestimates the load level significantly.

The discrepancy between yield line theory and test results is not surprising. First of all, the assumed deformation mode deviates from the actual one. Probably a considerable amount of energy is absorbed my membrane straining of bulkheads and stringers.

The other factor is the dynamic nature of the experiments. Inertia forces may introduce a deformation pattern differing from the static one. The strain rate sensitivity is also important. A rough estimate suggests that the dynamic increase in yield strength might well have exceeded 50%.

4. RESIDUAL STRENGTH OF DAMAGED BRACING ELEMENTS

4.1 General

The present section deals with axial strength of tubular members with damage in the form of local denting. The theoretical background of an efficient computer program for solving such problems is presented and comparison is made between analysis and test results on pin-ended columns.

A tubular member that has been dented without bending has local eccentricity in the dented region as well as additional residual stresses. The influence on the buckling load of these additional local imperfections is expected to be small, since buckling is an overall phenomenon of the whole member. However, the plastic collapse load of the member may be reduced to a value much lower than the buckling load, depending on the geometry of the dent and the properties of the member.

The behaviour of the dented member stressed until its ultimate strength may be divided into two phases.

Phase 1: Dent plastification.

When a small axial compressive load is applied to a dented tubular member, axial compressive stresses develop in the tube shell. At the dent these stresses are supported by compression and bending of the dented shell.

Considering the dented region, as shown in Fig. 20, axial compressive strain and bending deformation occur. Bending deformation which takes place mainly in the short flattened part at the middle of the dented shell is restrained by the rest of the tube and may be neglected. Only axial compressive strain is considered. As a result of this simplification, uniform shortening of the tube takes place and axial compressive stresses develop uniformly in the tube shell. In the dent, bending stresses are superimposed. As the axial load increases, yielding starts at the middle of the dent. Yielding continous until a full plactic hinge line is formed as shown in Fig. 20. Integrating the full plastic stress distribution at the middle of the dent and considering the equilibrium of the dented portion, the following expression is obtained

$$\sigma_{dp} = \sigma_y[\sqrt{4(\eta/t)^2 + 1} - 2(\eta/t)] \quad (15)$$

where

σ_{dp} = The uniform compressive stress in the tube shell when a full plastic hinge line is formed at the middle of the dent.

σ_y = the yield stress of the material,

η = as defined in Fig. 20 and

t = the thickness of the tube shell.

The axial compressive load acting on the tube at this time, P_{dp}, may then be given by

$$P_{dp} = P_p[\sqrt{4(\eta/t)^2 + 1} - 2(\eta/t)] \quad (16)$$

where

P_p is the full plastic compressive strength of the tubular member under consideration.

Phase 2: Ultimate Strength.

After plastification at the middle of the dent, the stiffness of the dented region is reduced to a large extent. Increment ΔP of the axial load P above the value P_{dp} of Eq. (16) is supported in the dented part of the tube primarily by the arc $\pi D-S$ in Fig. 20. In the parts of the tube from its ends to close up to the dent, the axial force is supported by the total cross-section. Adjacent to the dent, the axial stresses acting in the fibers which pass through the dent are transferred gradually to the arc $\pi D-S$ by the action of longitudinal shear in the tube shell. Thus, the eccentricity of the load increment starts to grow gradually a short distance before the dent to a maximum value at the middle of the dent and decrease again until it vanishes a short distance after the dent. This distance is dependent on the material of the tube and the proportions of the tube and the dent. The bending moment M_e caused by this eccentricity may then have a distribution as that shown in Fig. 21. A further simplification is obtained when a uniform distribution of M_e along the dent is assumed as shown in Fig. 21. M_e is given by

$$M_e = \Delta P a \quad (17)$$

where

a is the distance between the line of ΔP (center line of the tube) and the center of the area of the arc $\pi D-S$.

The bending moment M_e causes an overall bending of the member which is magnified by the axial load.

The deflection curve resulting from the moment M_e without the effect of the axial load is shown in Fig. 21. The part along the dent is an arc of a circle with radius ρ, since the moment M_e is assumed constant along the dent. The rest is straight lines since there is no bending moment acting in these regions.

The bending equation may be written as

$$\frac{E}{\rho} = \frac{Me}{I^*} \quad (18)$$

where

E is the modulus of elasticity.

I* the 2nd moment of area of the arc $\pi D-S$ about its neutral axis.

The deflection, δ_b, at the middle of the dent may be found approximately from the geometry as

$$\delta_b \simeq \ell_1\theta_1 \simeq \ell_2\theta_2 \quad (19)$$

where

θ_1, θ_2, θ_1 and ℓ_2 are defined in Fig. 21

The relation between the bending radius ρ and the angles of slope at the ends, θ_1 and θ_2 may be found from geometry in terms of the length of the dent, θ_d, as

$$\ell_d = \rho(\theta_1 + \theta_2) \tag{20}$$

Eqs. (17, 18, 19 and 20) yield expression for δ_b

$$\delta_b = \ell_1 \ell_d a\Delta P/[EI^*(1+\ell_1/\ell_2)] \tag{21}$$

Taking the magnifying effect of the axial force into account, the deflection at the middle of the dent may be expressed as

$$\delta = \delta_b \cdot mf \tag{22}$$

where

mf is the magnification factor,

$$= 1-\gamma(1-c)/(1-\gamma) \tag{23}$$

$$\gamma = (P_{dp}+\Delta P)/P_E \tag{24}$$

P_E is the Euler buckling load,

c is a geometrical factor

$$= [\ell/2\ell_2+\ell_d)] \cdot \sin[\pi(\ell_1+\ell_d/2)/\ell] \tag{25}$$

The total bending moment acting on the arc πD-S at the middle of the dent is then given by

$$M = \Delta P(a+\delta)+P_{dp}\delta \tag{26}$$

The stress distribution across the tube at the middle of the dent may be assumed linear across the arc πD-S as shown in Fig. 22.

The stress σ at the fibers adjacent to the dent is the sum of the uniform stress σ_{dp}, given by Eq. (15), the compressive stress σ_c caused by the force ΔP, and the bending stress σ_b caused by the bending moment M of Eq. (26), as shown in Fig. 22.

$$\sigma = \sigma_{dp} + \sigma_c + \sigma_b \tag{27}$$

When the fibers adjacent to the dent start to yield, the stiffness of the dented region decreases rapidly. As the lateral deflection develops, not much increase of the axial load is expected and the ultimate strength may be considered to be reached at this time. Denoting the load increment ΔP at this time by ΔP_U, Eq. (27) yields the following expression

$$\Delta P_U\left(\frac{1}{A^*} + \frac{a+\delta_U}{Z^*}\right) + P_{dp}\frac{\delta_U}{Z^*} = \sigma_y - \sigma_{dp} \tag{28}$$

where

A* is the cross-sectional area of the arc πD-S,

Z* is the modulus of section of the arc πD-S, and

δ_U is the lateral deflection at the dent when the ultimate strength is reached, as given by Eq. (22).

δ_U is a function of ΔP_U and Eq. (28) may be solved for ΔP_U and δ_U by iteration.

The ultimate compressive strength P_U is then given by

$$P_U = P_{dp} + \Delta P_U \tag{29}$$

4.2 Post-Ultimate Strength Behaviour

After the member has reached its ultimate strength, a more complicated behaviour of the dented part of the tube takes place. However, it may be assumed that the axial load remains almost constant for some time. The increase of the bending moment at the location of the dent due to the increasing lateral deflection is more or less overcome by the increasing capacity of the arc $\pi D-S$ to form a full plastic hinge. As lateral deflection increases, the axial load obviously starts to decrease before a full plastic hinge is formed. However, it is assumed that the plastic hinge is formed at the ultimate value of the axial load. Also as the lateral deflection increases, the dent starts to grow deeper in the tube shell. This growth is rather slow in the deformation range of interest for this study /24/ and the effect on the strength of the cross-section may be neglected. The ultimate strength interaction relationship of the axial load to the bending moment at the dent may then be simply constructed according to Fig. 23. This interaction relationship may be considered as plastic potential and a plastic hinge may be inserted in the location of the dent /25/.

The incremental load-deformation relationship of the member, with plastic hinge inserted, may now be constructed in the form of a stiffness matrix. Load increments (negative) may be applied in steps and the corresponding deformation obtained.

In order to obtain the stiffness matrix in its incremental form after a plastic hinge is formed at the dent, the member is divided at the middle of the dent into two beam-column elements. Three degrees of freedom is allowed at each nodal point as shown in Fig. 24. The elastic nonlinear stiffness matrix of each element is established. The form of this stiffness matrix may be found in standard texts /26/. In this stiffness matrix the effect of bending deflection on axial deformation is not considered. Having these two matrices the tangential forms are derived. Then a plastic hinge is inserted at the position of the dent in one element and the tangential elastic-plastic stiffness matrix of this element is derived according to the plastic flow theory following the formulation presented by Ueda et al. /27/. The two elements are then assembled to obtain the global stiffness matrix. As deformation increases some nonlinear terms which are neglected in the elastic stiffness matrix become larger. They are included by establishing a global system of axes and a local one for each element. The local systems are updated after each load step.

4.3 Computer Program

A computer program, DENTA, has been developed to perform the analysis. Examples of results are presented in Fig. 8. Ultimate load and accompanying deformations are calculated analytically while the post-ultimate strength behaviour is calculated numerically as explained in preceeding sections. The load and deformation in each case have been traced in the post-ultimate strength range from the ultimate load down to 0.2 of its value in about 20 steps. A UNIVAC 1108 computer was used for the analysis. Computer time has been recorded less than 0.8 second (CPU) per tube.

4.4 Experimental and Numerical Investigation

Axial compression tests were carried out on a series of 21 tubes after dented. The aim of the tests was to gain a better understanding of the behaviour of dented tubular members. The analytical model is based on this understanding and checked agains the results of the tests.

The tests were carried out on DIN 2391 ST 35 BK high precision tubes. Dimensions, summarized in Table 1, were chosen to represent, to scale, the range of tubes usually met in offshore practice. The tubes were stress relived in order to eliminate unknown residual stresses by heating to 550° for one hour followed by slow cooling.

Following heat treatment, test tubes were cut and machined at the ends. Two or three tensile test specimens were cut from each tube. Thickness, circularity and material properties of tubes were then surveyed. Thickness was measured at 20 points on each tube using an ultrasonic transducer. The measurements were checked against micrometer readings at the ends of test tubes. Outer diameters are measured at 5 stations along each tube, 4 diameters spaced at 45 degrees are measured at each station.

Tensile tests was carried out under displacement control at a strainrate of about 3×10^{-7}/sec. Average values of the results are summarized in Table 5 together with geometric properties.

Test tubes are then dented at 3/8th of their length in order to differentiate between buckling collapse, and plastic collapse at the dent. Denting was carried out in a hydraulic press through a knife edge with 5 mm noze radius. The back of each tube was supported in a cylindrical wooden bed having the same diameter as the tube in order to prevent lateral deflection of the tube

as far as possible. After denting, the straightness of each tube was measured optically in the x-z plane, see Fig. 25. Results are summarized in Table 5. Each tube was fitted at its ends with sliding fit steel plugs to prevent premature local buckling at the ends and spherical heads of hardened high strength steel to simulate simple supports. Axial compressive load was applied under displacment control at an average strain rate of about 3×10^{-7} using an electronically controlled hydraulic jack of 2500 kN capacity through a calibrated load cell. End shortening, lateral deflection in x-direction at the dent and the growth of the dent were continously recorded at about 10 seconds intervals by displacement transducers. Displacement signals were automatically translated and printed out.

Strains at stations 2D from each end and at midlength were measured. Three electric strain gauges at 120^{o} were fitted at each section. Axial load and bending moment were automatically calculated from strain measurements and printed out together with those obtained from the load cell and deflection measurements. The load, measured by the load cell, is plotted against end shortening on an X-Y plotter.

Results of these are summarized in Table 5 and Fig. 26 together with theoretical results calculated by the present theoretical model. Typical load shortening curves are presented in Fig. 27. Satisfactory agreement of results of analysis by the present model with those of the tests exists for the ultimate load as well as the post-ultimate strength behaviour.

5. CONCLUSIONS

Simple methods to estimate the energy absorption characteristics of tubular steel members of platforms and ship bows have been assessed by comparison with experiments.

In tubular members energy is dissipated due to the local denting at the loaded part of the member and overall hinge mechanism of the actual member. Up to now the methods developed have been based on plastic mechanisms, neglecting local effects. This initial work has also been limited to the members themselves, without considering explicitly the behaviour of the tubular joints where crippling or brittle fracture might significantly affect the energy absorption properties. Simple methods for collapse analysis of tubular beams have been modified so as to reproduce the behaviour predicted by experiments and refined numerical techniques.

Analytical expressions for the energy absorption in cylindrical shells for various collapse modes have been outlined and related to the collision behaviour of bulbous bows. A series of tests on ring-stiffened cylinders under static and dynamic loading have been described and compared with analytical solutions. Some discrepancy is found between analysis and test results, and in all cases the analytical methods come out to be conservative in the sense that they give capacities below the experimental values.

A simple numerical model for predicting post-damage strength of dented tubular members has been outlined. Good agreement is obtained with experimental studies and the computer time requirement for the analysis is extremely short. The technique has proven to be an efficient tool for checks of individual dented tubular members.

The present work should be understood as an introductory study of ship/platform impacts. It is clear from the above considerations that future improvements in theoretical models must be accompanied by experimental verifications. In the study of deformation characteristics of ships all energy absorbing components must be taken into account including decks and bulkheads. For bracing elements special attention should be given to the performance of tubular joints under ultimate loading.

REFERENCES

/1/ Moan, T. and Holand, I., 1981, "Risk Assessment of Offshore Structures. Experience and Principles", Structural Safety and Reliability (ed. Moan and Shinozuka), Proceedings of ICOSSAR'81, Elsevier Scientific Publishing Company.

/2/ Costa, F. Vasco, 1964, "The Berthing Ship", The Dock and Harbour Authority, Vol. XLV.

/3/ Furnes, O. and Amdahl, J., 1980, "Ship Collisions with Offshore Platforms", Intermaritec, Hamburg.

/4/ Søreide, T.H., 1981, Ultimate Load Analysis of Marine Structures, Tapir Publishing Company, Trondheim, Norway.

/5/ Jones, N., 1976, "Plastic Behaviour of Ship Structures", Transactions Society of Naval Architects and Marine Engineers, Vol. 84, pp. 115-145.

/6/ Hodge, Ph.G., 1974, "Post-Yield Behaviour of a Beam with Partial End Fixity", International Journal of Mechanical Sciences, Vol. 16, pp. 385-388.

/7/ Sherman, D.R. and Glass, A.M., 1974, "Ultimate Bending Capacity of Circular Tubes", OTC 2119, pp. 901-910.

/8/ Sherman, D.R., 1976, "Tests of Circular Steel Tubes in Bending", ASCE J. Struct. Div., Vol. 102, No. ST11, pp. 2181-2195.

/9/ American Petroleum Institute, 1979, Recommended Practice for Planning, Designing and Constructing Fixed Offshore Platforms, API RP 2A.

/10/ Remseth, S.N., Holthe, K., Bergan, P.G. and Holand, I., 1978, "Tube Buckling Analysis by the Finite Element Method", Finite Elements in Nonlinear Mechanics, Tapir Publishing Company, Trondheim, Norway.

/11/ Søreide, T.H., 1977, Collapse Behaviour of Stiffened Plates using Alternative Finite Element Formulations, Dr.ing. Thesis, Division of Structural Mechanics, The Norwegian Institute of Technology, Trondheim, Norway.

/12/ Yura, J.A., Zettlemoyer, N. and Edwards, I.F., 1980, "Ultimate Capacity Equations for Tubular Joints", OTC 3690.

/13/ Det norske Veritas, 1977, Rules for the Design, Construction and Inspection of Offshore Structures.

/14/ Søreide, T.H. and Amdahl, J., 1982, "Energy Absorption in Bracings", Norwegian Maritime Research.

/15/ Odland, J., 1978, "Buckling Resistance of Unstiffened and Stiffened Circular Cylindrical Shell Structures", Norwegian Maritime Research, Vol. 6, No. 3, pp. 2-22.

/16/ Alexander, H.M., 1960, "An Approximate Analysis of the Collapse of Thin Cylindrical Shells Under Axial Loading", Quart. Journal of Mech. Appl. Math., Vol. XIII, No. 4.

/17/ Johnson, W., Soden, P.D. and Al-Hassani, S.T.S., 1977, "Inextensional Collapse of Thin-Walled Tubes Under Axial Compression", J. Strain Analysis, Vol. 12, No. 4.

/18/ Cowper, G.R. and Symonds, P.S., 1957, Strain Hardening and Strain Rate Effects in the Impact Loading of Cantilever Beams, Brown Univ. Techn., Report No. 28.

/19/ Wierzbicki, T. and Abramowicz, W., 1979, "Crushing of Thin-Walled Strain Rate Sensitive Structures", paper presented at Euromech Colloquium No. 121.

/20/ Odland, J., 1981, On the Strength of Welded Ring Stiffened Cylindrical Shells Primarily Subjected to Axial Compression, Dr.Ing. Report, Division of Marine Structures, The Norwegian Institute of Technology, Trondheim.

/21/ Woisin, G., 1976, "Die Kollisionsversuche der GKSS", Jahrbuch der Schiffbautechnischen Gesellshaft, 70.8, Hamburg.

/22/ Minorsky, V.U., 1977, Bow Loading Values (Bulbous Bow), U.S. Mar. Ad., Dept. of Commerce, Washington, Rep. MA-RD-920-78035.

/23/ Gerard, G., 1957, "The Crippling Strength of Compression Elements", Am. Inst. of Aeronautics and Astronautics, May 1957.

/24/ Taby, J. and Rashed, S.M.H., 1980, Experimental Investigation of the Behaviour of Damaged Tubular Members, Division of Marine Structures, Norwegian Institute of Technology, Trondheim.

/25/ Taby, J., Moan, T. and S.M.H. Rashed, 1981, "Theoretical and Experimental Study of the Behaviour of Damaged Tubular Members in Offshore Structures", Norwegian Maritime Research, Vol. 9, No. 2.

/26/ Livesley, R.K., 1975, Matrix Methods of Structural Analysis, Pergamon Press.

/27/ Ueda, Y. et al., 1967-1968, Elastic-Plastic Analysis of Framed Structures Using the Matrix Method, 1st and 2nd reports. Journal of the Society of Naval Architects of Japan. Vols. 124 and 126. (In Japanese).

SPECI-MEN	OUTER DIAMETER (mm)	WALL THICKNESS (mm)	D/t	LENGTH (mm)	L/d	YIELD STRESS (N/mm^2)
IAI	125.15	2.04	61.33	1244.3	9.94	204
IAII	125.13	2.04	61.34	1245.9	9.96	211
IAIII	125.19	2.04	61.37	1244.8	9.94	207
IBI	125.14	2.50	50.06	1244.9	9.95	251
IBII	125.19	2.51	49.88	1245.8	9.95	230
IBIII	125.11	2.50	50.04	1245.5	9.96	268
ICI	125.11	3.07	40.75	1245.9	9.96	260
ICII	125.14	3.10	40.37	1240.5	9.91	328
ICIII	125.09	3.06	40.88	1246.6	9.97	256
IDI	114.5	3.25	35.23	1240.5	10.83	235
IDII	114.5	3.25	35.23	1240.5	10.83	235
IEI	88.5	3.0	29.50	1240.5	14.02	235
IEII	88.5	3.0	29.50	1240.5	14.02	235
IFI	63.4	2.9	21.86	1240.5	19.57	235
IFII	63.4	2.9	21.86	1240.5	19.57	235

Table 1. Data for bracing models.

Test specimen	MA1	MA2	MA3	MA4	FA1	FA2	FA3	FA4	FA5	FA6
Wall thickness t mm	0.97	1.22	0.99	0.98	2.03	2.06	2.06	2.04	2.05	2.05
Stiffener spacing ℓ mm	23.0	37.0	33.5	33.5	47.0	57.0	67.0	97.0	117.0	
Yield stress σ_y N/mm^2	267	267	267	267	236	236	236	228	228	228

Table 2. Wall thickness and stiffener spacing for ringstiffened cylinders.

Test specimen	MA1	MA2	MA3	MA4	FA1	FA2	FA3	FA4	FA5	FA6
Theoretical solution N/mm^2	224	218	202	204	222	220	200	205	206	206
Experimental results N/mm^2	259	293	260	267	142	230	247	261	135	209

Table 3. Initial buckling stresses for ringstiffened cylinders.

Test specimen	MA1	MA2	MA3	MA4	FA1	FA2	FA3	FA4	FA5	FA6
Experiments MN	68.1	103.2	80.5	62.5	158.2	147.8	143.6	139.9	147.4	101.4
Static theory	55.0	65.7	48.8	48.8	111.8	109.3	107.3	112.5	124.8	71.7
Static theory/Exper.	0.81	0.64	0.61	0.78	0.71	0.74	0.75	0.80	0.85	0.71
Dynamic theory/Exper.	0.93	0.73	0.69	0.89	0.80	0.83	0.84	0.90	0.96	0.81

Table 4. Analytical and experimental values for average load P_{av} for ringstiffened cylinders.

Specimen No.	Outer-Diameter D mm		Thickness t mm		Length L mm	Young's Modulus E N/mm² x10⁵	Yield stress σ_y N/mm²	$\frac{D}{t}$	$\frac{L}{r}$	λ	Max. Deviation from straightness δ_0/L	Depth of Dent DD mm	$\frac{DD}{D}$	Buckling[3] Load (Undamaged) σ_u/σ_y	Theoretical max. load σ_u/σ_y	Experimental max. load σ_u/σ_y
	mean	cov.	mean	cov.												
I A I	125.145	.00111	2.04	.02875	3500	1.88	204	61.3	80.40	0.839	.00074	6.25	.050	.834	.635	.667
I A II	125.127	.00082	2.04	.03071	"	1.96	211	61.3	80.42	0.839	.00183	12.6	.101	.834	.476	.529
I B I	125.138	.00071	2.50	.03030	"	2.11	250	50.1	80.70	0.885	.00054	6.3	.050	.811	.641	.638
I B II	125.191	.00110	2.51	.03183	"	1.98	230	49.9	80.68	0.874	.00151	12.5	.100	.816	.484	.528
I C I	125.107	.00045	3.07	.01503	"	2.01	290	40.8	81.09	0.981	.00057	6.25	.050	.756	.647	.656
I C II[1]	125.136	.00059	3.095	.03470	"	1.98	328	40.4	81.09	1.050	.00206	12.25	.098	.713	.484	.505
II A I	160.202	.00181	2.525	.01881	"	2.00	351	63.4	62.78	0.838	.00023	8.00	.050	.835	.631	.683
II A II	160.161	.00136	2.52	.02220	"	1.97	392	63.6	62.79	0.874	.00166	16.08	.100	.816	.471	.437
II A III	160.171	.00132	2.525	.01720	"	1.94	314	63.4	62.79	0.773	.00106	3.2	.020	.865	.801	.731
II B I	160.162	.00138	3.06	.03135	"	1.94	330	52.3	63.00	0.795	.00120	7.9	.049	.855	.643	.544
II B II	160.141	.00054	3.075	.03452	"	1.94	233	52.1	63.02	0.668	.00194	16.0	.100	.908	.488	.548
II B III	160.089	.00059	3.065	.02765	"	1.94	258	52.2	63.03	0.721	.00051	3.2	.020	.807	.816	.796
II C I	160.110	.00050	4.065	.01443	"	1.96	470	39.4	63.42	0.979	.00091	8.6	.054	.758	.629	.607
II C II	160.230	.00092	4.10	.04293	"	2.01	457	39.1	63.38	0.985	.00217	16.1	.100	.754	.483	.478
II C III[2]	160.074	.00084	4.07	.01457	"	1.92	384	39.3	63.44	0.885	.00077	3.15	.020	.811	.833	.791
III A I	250.259	.00045	4.23	.01936	"	2.02	500	59.2	40.23	0.639	.00060	12.6	.050	.917	.638	.595
III A II	250.225	.00055	4.27	.02191	"	2.02	502	58.6	40.24	0.638	.00100	25.5	.102	.918	.477	.463
III B I	250.245	.00096	5.20	.02003	"	2.00	470	48.1	40.39	0.625	.00010	13.6	.054	.923	.632	.714
III B II	250.257	.00132	5.21	.01960	"	1.97	433	48.0	40.39	0.603	.00200	26.0	.104	.930	.481	.533
III C I	250.373	.00112	6.02	.02271	"	1.98	472	41.6	40.67	0.629	.00087	12.6	.050	.922	.657	.734
III C II	250.457	.00201	6.00	.01659	"	2.02	465	41.7	40.65	0.624	.00183	25.0	.100	.923	.495	.556

(1) Collapse started at the dent but continued at a different location.
(2) The theoretical max. load is higher than the buckling load. The tube buckled outside the dent as expected.
(3) The buckling load is calculated by table 14.2 and Fig. 14.10 (a), Chen, W.F. and Atsuta, T., Theory of Beam Columns, Vol. 1, McGraw-Hill Inc.

Table 5. Summary of tests on residual strength of tubular members.

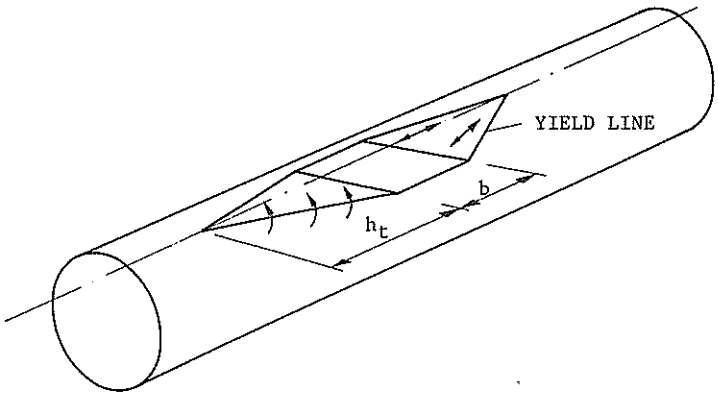

Fig. 1 Plastic mechanism for sideways impact by supply vessel on jacket leg.

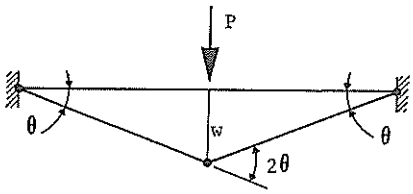

Fig. 2 Collapse mechanism for bracing element.

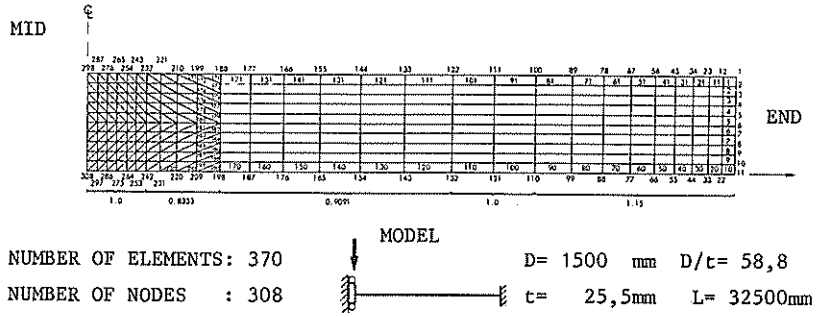

Fig. 3 Finite element shell model of bracing element.

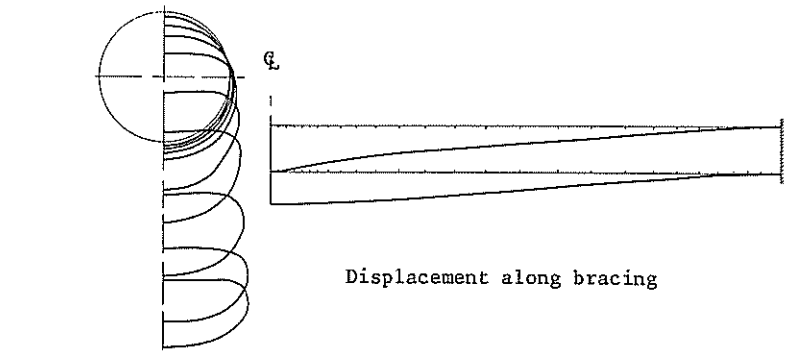

Fig. 4 Deformation patterns from shell analysis.

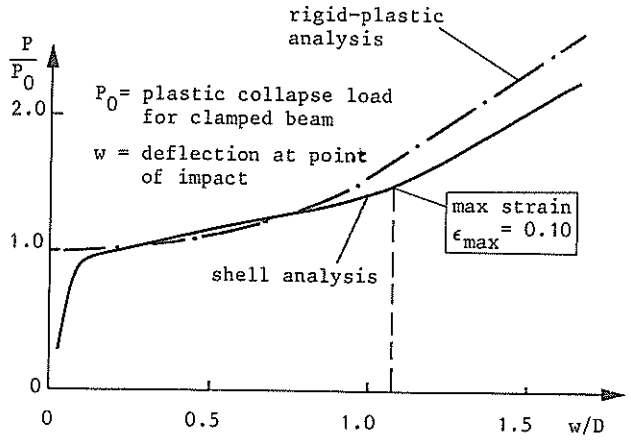

Fig. 5 Load-displacement relation for bracing element. Finite element shell analysis.

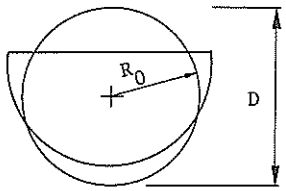

Fig. 6 Deformation model of cross-section at point of impact for calculating reduced section modulus.

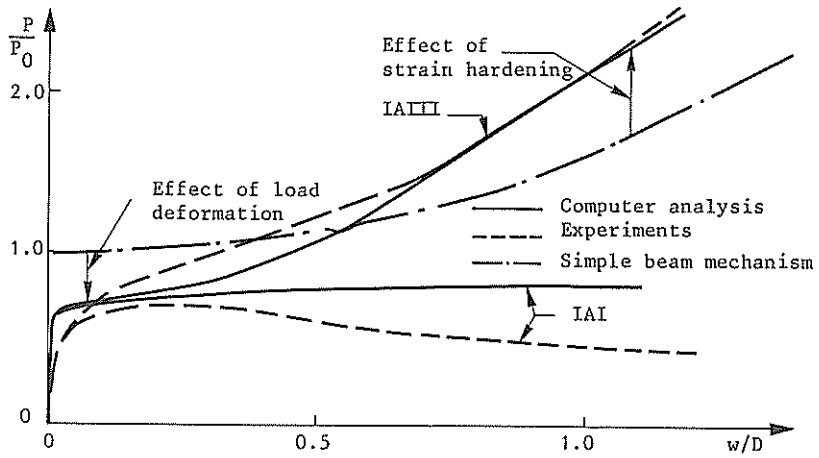

Fig. 7 Load-deflection characteristics for specimens IAI and IAIII.

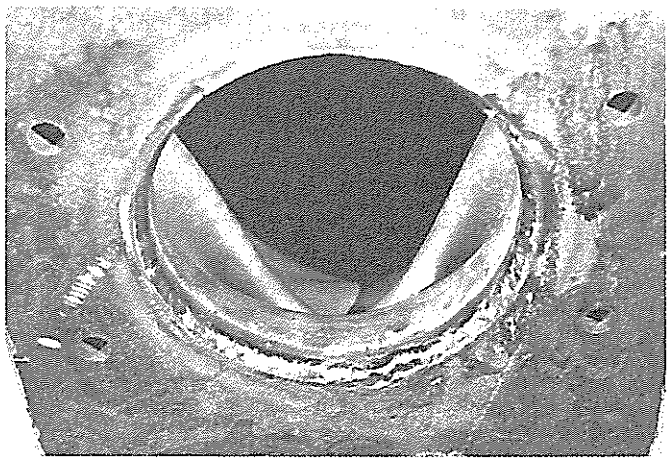

Fig. 8 Local crippling of tube wall at end of specimen IAI.

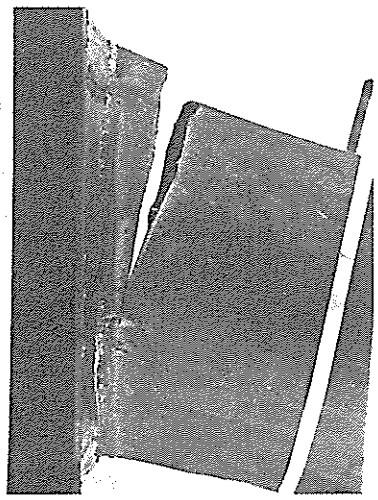

Fig. 9 Fracture at end of specimen IAIII.

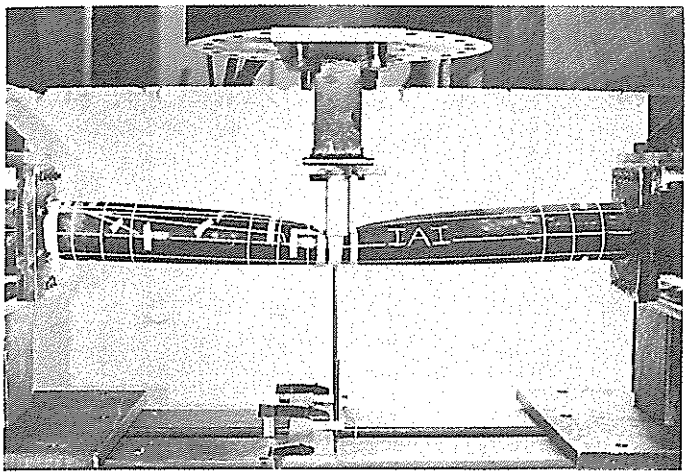

$P/P_0 = 0.67$

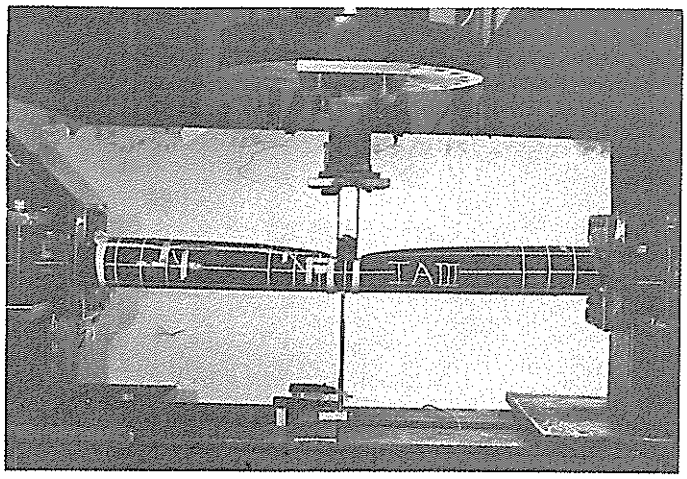

$P/P_0 = 0.63$

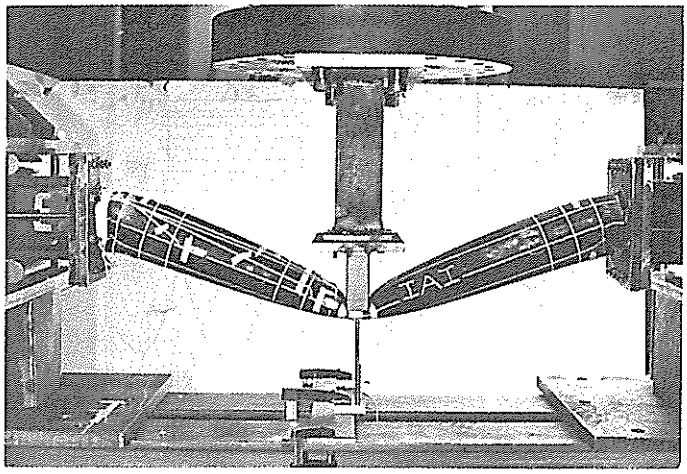

$P/P_0 = 0.53$

Fig. 10 Deformation of horizontally free specimen IAI.

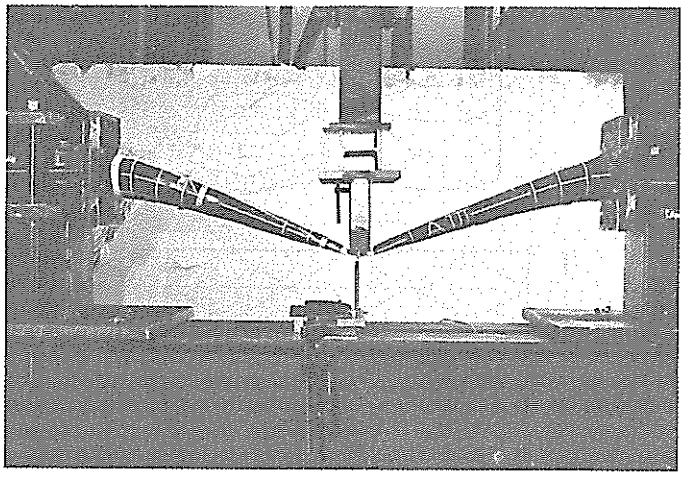

$P/P_0 = 3.41$

Fig. 11 Deformation of horizontally fixed specimen IAIII.

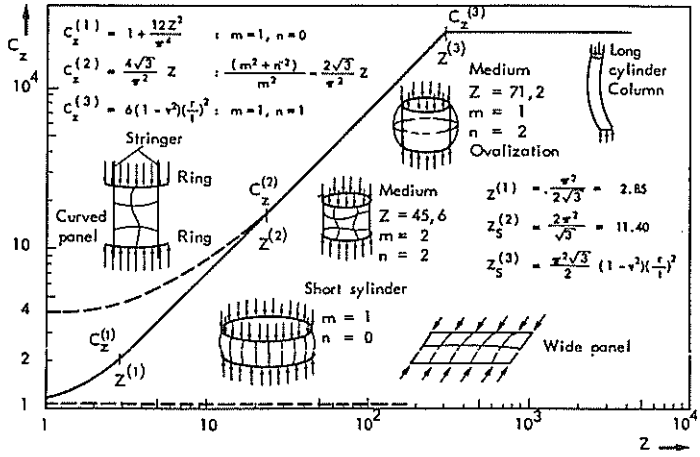

Fig. 12 Buckling coefficients for ring-stiffened cylinders.

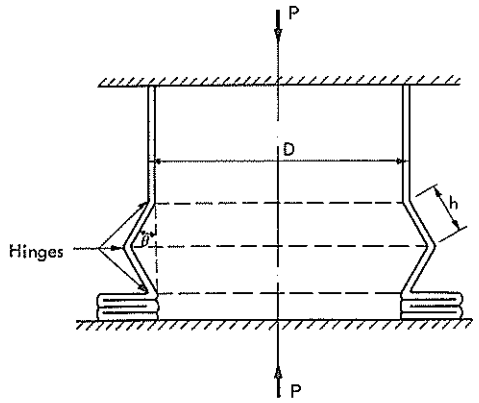

Fig. 13 Axisymmetric collapse model for ring-stiffened cylinder.

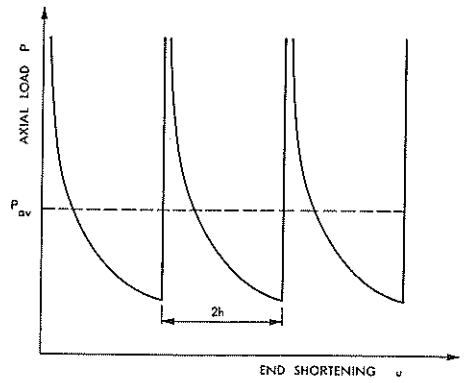

Fig. 14 Theoretical load-displacement curve for ring-stiffened cylinder.

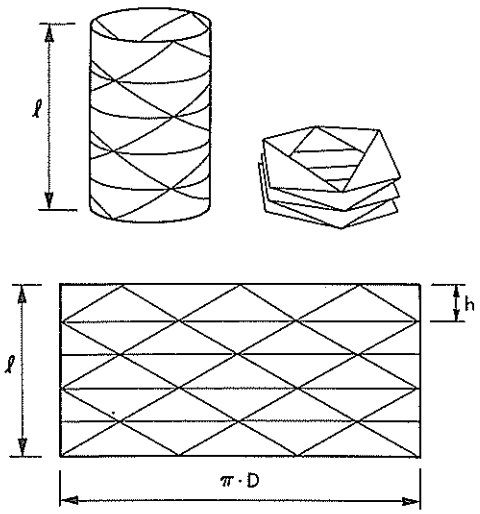

Fig. 15 Asymmetric collapse model for cylindrical shell.

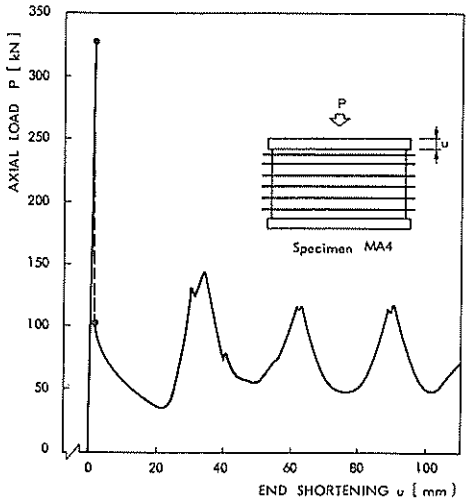

Fig. 16 Load-displacement curve for specimen MA4.

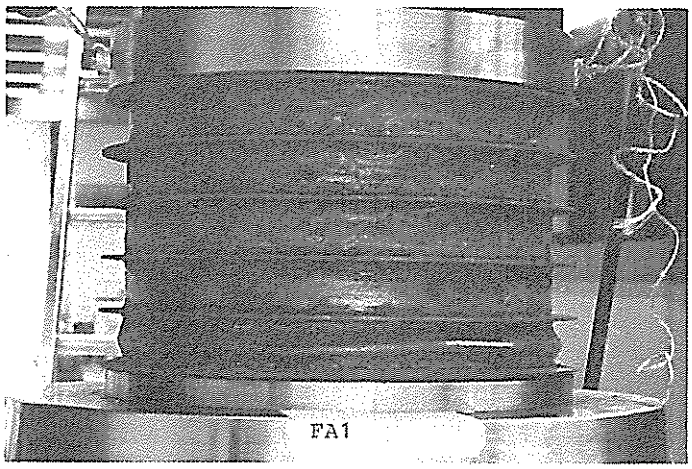

u = 10 mm

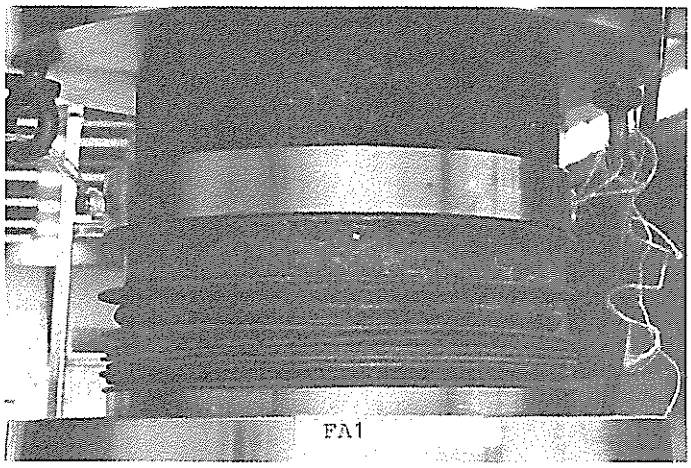

u = 120 mm

Fig. 17 Axisymmetric collapse of specimen FA1.

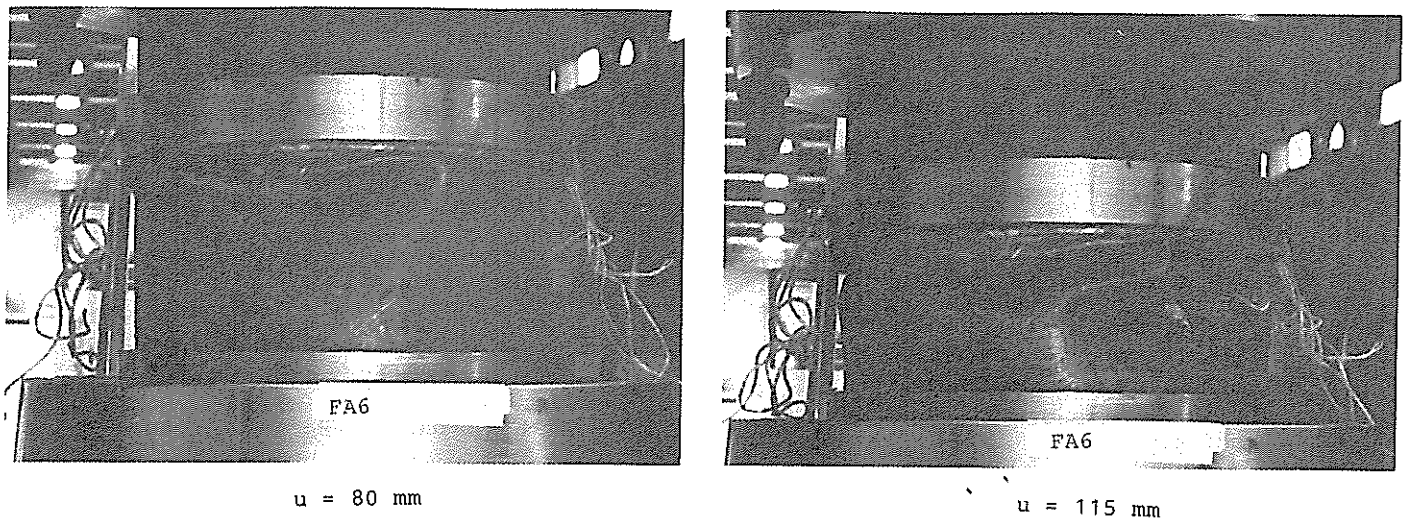

u = 80 mm

u = 115 mm

Fig. 18 Asymmetric collapse of specimen FA6.

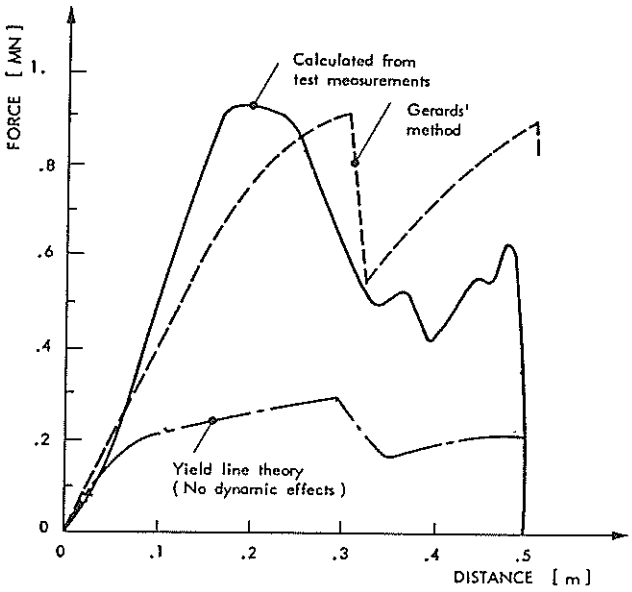

Fig. 19 Comparison between experiments and theory on tanker bow model.

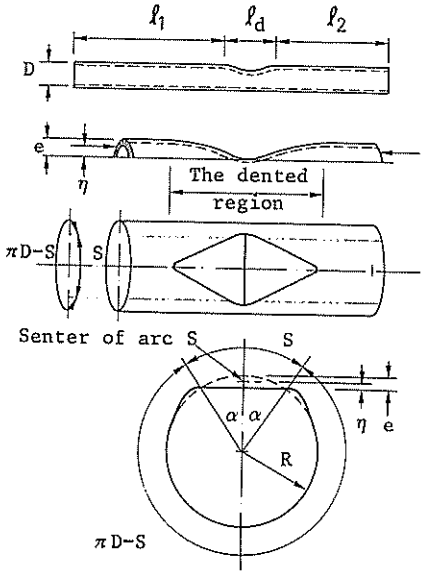

Section through the middle of the dent

Fig. 20 The dented tubular member.

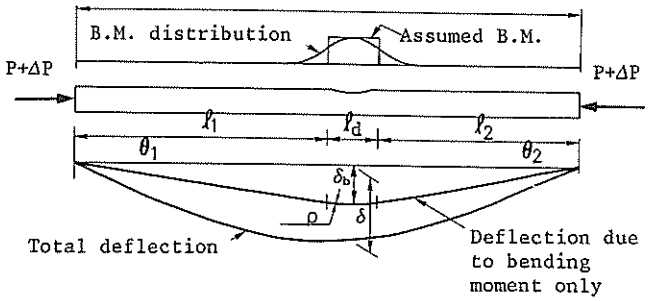

Fig. 21 Bending moment and deflection curves.

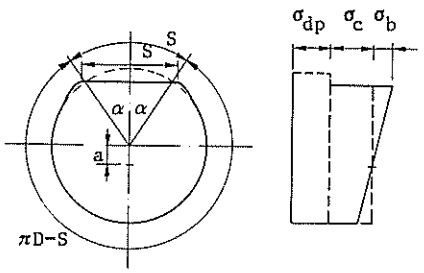

Fig. 22 Stress distribution at dented region during phase II.

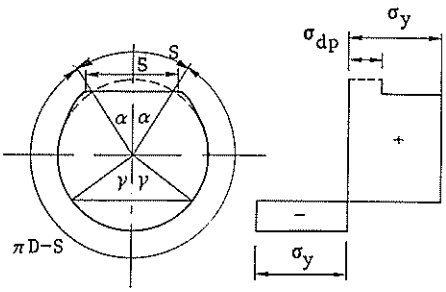

Fig. 23 Assumed stress distribution at ultimate strength of dented region.

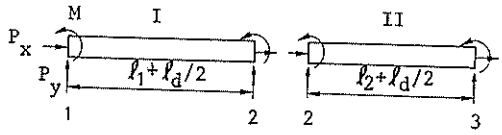

Fig. 24 Beam-column elements with parameters.

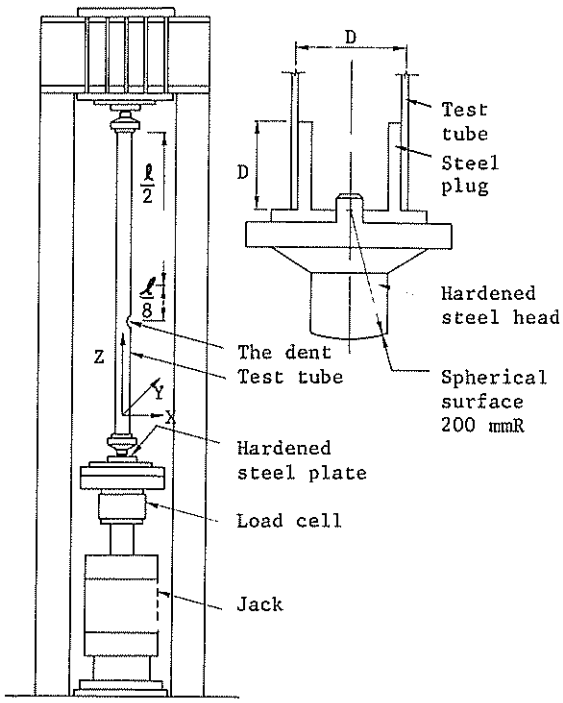

Fig. 25 General arrangement of test rig and tube head arrangement.

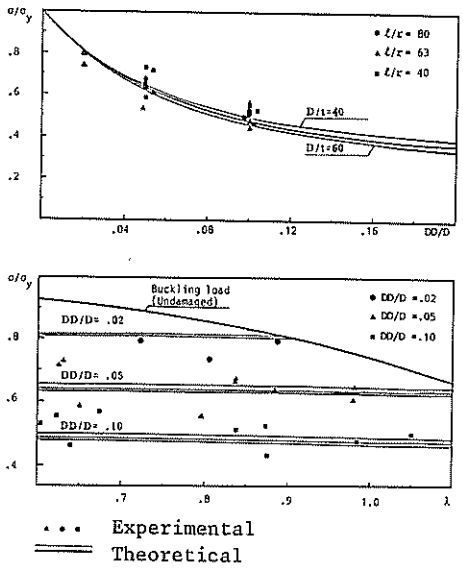

Fig. 26 Theoretical and experimental values on ultimate loads.

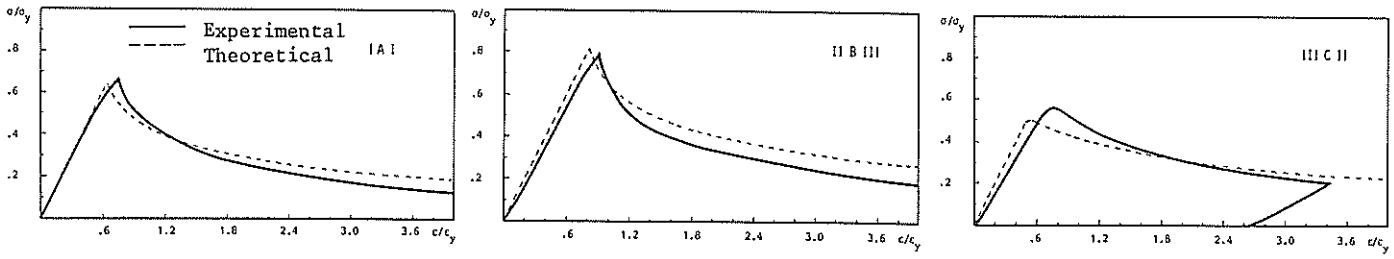

Fig. 27 Typical load-shortening curves.